Cronfa - Swansea University Open Access Repository

Estimating Forest Canopy Parameters From Satellite Waveform LiDAR by Inversion of the FLIGHT Three-Dimensional Radiative Transfer Model

I. J. Bye[a], P. R. J. North[a], S. O. Los[a], N. Kljun[a], J. A. B. Rosette[a], C. Hopkinson[b], L. Chasmer[b], C. Mahoney[b]

[a]*Global Environmental Modelling and Earth Observation (GEMEO), Department of Geography, Swansea University, SA2 8PP, United Kingdom*
[b]*Department of Geography, University of Lethbridge, 4401 University Drive, Lethbridge, Alberta T1K 3M4*

Abstract

The Geoscience Laser Altimeter System (GLAS) has the potential to accurately map global vegetation heights and fractional cover metrics using active laser pulse emission/reception. However, large uncertainties in the derivation of data products exist, since multiple physically plausible interpretations of the data are possible. In this study a method is described and evaluated to derive vegetation height and fractional cover from GLAS waveforms by inversion of the FLIGHT radiative transfer model. A lookup-table is constructed giving expected waveforms for a comprehensive set of canopy realisations, and is used to determine the most likely set of biophysical parameters describing the forest structure, consistent with any given GLAS waveform. The parameters retrieved are canopy height, leaf area index (LAI), fractional cover and ground slope. The range of possible parameters consistent with the waveform is used to give a per-retrieval uncertainty estimate for each retrieved parameter. The retrieved estimates were evaluated first using a simulated data set and then validated against airborne laser scanning (ALS) products for three forest sites coincident with GLAS overpasses. Results for height retrieval show mean absolute error (MAE) of 3.71 m for a mixed temperate forest site within Forest of Dean (UK), 3.35 m for the Southern Old Aspen Site, Saskatchewan, Canada, and 5.13 m for a boreal coniferous site in Norunda, Sweden. Fractional cover showed MAE of 0.10 for Forest of Dean and 0.23 for Norunda. Coefficient of determination between ALS and GLAS estimates over the combined dataset gave R^2 values of 0.71 for height and 0.48 for fractional cover, with biases of -3.4 m and 0.02 respectively. Smallest errors were found where overpass dates for ALS data collection closely matched GLAS overpasses. Explicit instrument parameterisation means the method is readily adapted to future planned spaceborne LiDAR instruments such as GEDI.

Keywords:

1. Introduction

Satellite laser altimeters have the capacity to provide global estimates of vegetation height and structure (Lefsky, 2010; Simard et al., 2011; Los et al., 2012). This can provide an important baseline for future assessment and comparison of forest structural changes, including biomass. Such estimates are needed to inform and test models of carbon sequestration (Ciais et al., 2013), and to monitor changes in carbon stocks due to climatic change and both natural and human disturbance (Goetz and Dubayah, 2011).

While passive optical systems have been used extensively to observe vegetation covered land by measuring the spectral properties of the surfaces, such systems are limited in their ability to measure vertical structure below the upper surface of the canopy. Active light detection and ranging (LiDAR) systems have addressed this, providing information about the vertical profile of a forest canopy. Waveform LiDAR has been in use since the early 1980s, when the Wallops Flight Facility's AOL airborne laser scanner was used to profile a 14 km flight line near Doubling Gap, Pennsylvania (Nelson et al., 1984). Height and density metrics were compared with photogrammetry derived values and the results were encouraging; height means were within 0.6 m of their respective photointerpreted values. Aldred et al. (1985) also demonstrated that waveform recording LiDAR had the potential to mitigate one of the problems arising from the use of discrete-return LiDAR, which was the systematic underestimation of stand height. In the 1990s, first Scanning LiDAR Imager of Canopies by Echo Recovery (SLICER) (Means et al., 1999; Lefsky et al., 1999a,b; Harding et al., 2001) and then Laser Vegetation Imaging Sensor (LVIS) (Blair et al., 1999; Drake et al., 2002) were developed by NASA as demonstrators for potential spaceborne LiDAR.

In the decade following, the Geoscience Laser Altimeter System (GLAS), a space-borne waveform instrument, was carried on the ICESat mission (Brenner et al., 2003). While GLAS was primarily designed to measure ice sheet topography, secondary objectives included measurements of vegetation height and land surface elevation. Launched in January 2003, the mission lasted until October 2009 when its instrument failed. The mission platform was placed in a 183 day ground track repeat cycle, to provide a 15 km spacing between tracks at the equator and 2.5 km at 80° latitude. Using GLAS data, canopy height has been estimated directly from the Gaussian wave components of a decomposed LiDAR waveform (Harding and Carabajal, 2005; Lefsky et al., 2005, 2007; Rosette et al., 2009; Duncanson et al., 2010), and volume has also been successfully derived (Rosette et al., 2008a; Nelson et al., 2009; Popescu et al., 2011). More recently, near global datasets of height for forest (Lefsky, 2010; Simard et al., 2011) and total vegetation (Los et al., 2012) have demonstrated the importance of the near-global coverage of GLAS. Los et al. (2012) conclude that the GLAS height product appears to be better suited as an input to ecological and climate models than existing data sets based on land cover alone.

For the previous two decades, the use of LiDAR to map biomass has increased dramatically. It is likely that over the next decade, in combination with other forms of remote sensing, LiDAR will become increasingly central to mapping biomass at regional, national or continental scales (Goetz and Dubayah, 2011; Wulder et al., 2012; Neigh et al., 2013). In particular, upcoming space borne LiDAR missions, such as the Global Ecosystems Dynamics Investigation (GEDI) LiDAR (Dubayah et al., 2014; Coyle et al., 2015) and the second generation ICESat-2 (Abdalati et al., 2010; Montesano et al., 2015) will have the potential to improve and update a definitive baseline for global biomass stocks.

The complex structure of a vegetation canopy in combination with uncertainties arising from instrument, suggest that remote sensing of vegetation biophysical parameters is an ill-posed problem; that is, multiple interpretations of the measured radiative signal are possible. A physically based radiative transfer model (RTM) (e.g. (Sun and Ranson, 2000; Ni-Meister et al., 2001b; Disney et al., 2006; North et al., 2010)) can be used to describe the interaction of radiation with canopy elements and explicitly relate canopy parameters, observation and illumination variables and

remote sensing signature.

Model inversion may be considered a multi parameter optimisation problem. However iterative numerical optimisation methods tend to be computationally intensive, and may not be appropriate for applications on a per-pixel basis for regional and global data (Kimes et al., 2002). An efficient approach to model inversion is the lookup table (LUT) method. It involves: generating of a table of reflectance signatures by varying the values of a set of reflectance model input parameters, comparing an observed signal against all signatures in the LUT to determine the best fit and corresponding set of parameters. Unlike iterative optimisation based approaches, LUTs can be applied to computationally expensive and complex models without any modifications, and so are particularly suitable for Monte Carlo or ray tracing models such as the 3D radiative transfer model, FLIGHT, we have used in this study (Weiss et al., 2000; Leonenko et al., 2013). Also, unlike iterative methods, LUTs do not require a set of initial values, preventing the chance of poor values leading to non-global minima. The effectiveness of the LUT approach to model inversion is sensitive to the accuracy of the RT model, but also to assumptions concerning choice of LUT generation parameters and crown macro-structure and shape. Turbid medium geometric primitives are typically used to model LUT canopy realisations due to their simplicity. However, studies (Calders et al., 2013; Widlowski et al., 2014) suggest that biophysical parameter retrieval may be sensitive to choice of crown shape or internal structure, and further work is recommended to improve understanding of this.

Several studies have applied model inversion to airborne LiDAR waveform (Koetz et al., 2006, 2007; Ma et al., 2015). In particular LUTs have been used previously to invert LiDAR data with some success by Koetz et al. (2006), who inverted a 3D LiDAR waveform model (Sun and Ranson, 2000). Subsequently, Koetz et al. (2007) investigated the fusion of imaging spectrometer and LiDAR data, demonstrating greater constraint on LAI. The inversion was tested on both simulated data and waveform data synthesised from small-footprint data acquired in the Swiss National Park, showing good correlation with retrieved parameters.

Existing datasets of height derived from GLAS show higher disagreement for regions of dense forest cover and higher ground slopes (Los et al., 2012; Xing et al., 2010); a physically-based joint retrieval of slope, cover and height has potential to improve accuracy over such regions. Fractional cover has previously been estimated (Los et al., 2012) over wider regions by statistical sampling, assuming each footprint represents either zero or complete vegetation cover, rather than per-footprint. This study aims to develop and evaluate a model inversion method suitable for satellite LiDAR waveform observations, to retrieve simultaneously parameters such as maximum canopy height (H_{top}), fractional cover (F_c), underlying topography and estimates of their error. In the following sections we will describe a lookup table (LUT) based inversion of the three-dimensional radiative transfer model FLIGHT (North, 1996; North et al., 2010) and evaluate the retrieval using GLAS waveform data, validated against airborne laser scanning data.

3

2. Method

In this section we first describe the FLIGHT (North, 1996; North et al., 2010) radiative transfer model applied to simulation of GLAS waveforms. We next outline generation of a lookup table for performing model inversion. Finally we describe the method for determining the most likely set of biophysical parameters describing the forest structure for a given waveform, and error estimates associated with these parameters.

2.1. FLIGHT Radiative Transfer Model

The FLIGHT radiative transfer model simulates vegetation bidirectional reflectance and LiDAR return by applying Monte Carlo simulation of photon transport within a three dimensional representation of vegetation structure. In the original radiative transfer mode of operation of FLIGHT (North, 1996), photon trajectories are traced forwards from the source, through a sequence of interactions between and within crown boundaries. At each interaction a photon may be absorbed, reflected or transmitted and this process is modelled with a continuous probability density function. On leaving the canopy boundary, energy is accumulated in bins defined for each solid angle of exit. The LiDAR mode of the model (North et al., 2010) samples the paths of individual photons received within the field of view of a given sensor position, accumulating path length and energy from both laser and solar sources and including multiple scattering events.

Large-scale forest structure is modelled by a set of geometric primitives, either ellipsoidal or conical, giving approximate extent of foliage vertical and horizontal extent. The representation is widely used to allow modelling of the main characteristics of three-dimensional forest canopies, but which remains computationally tractable by allowing a semi-analytic radiative transfer approach (Ni-Meister et al., 2001a; Duursma et al., 2012; North, 1996). A simple growth model is used to limit the degree of overlap between neighbouring crowns. Inside each crown, foliage is modelled using the parameters of leaf area density, leaf angle distribution (LAD), size and the optical parameters of reflectance and transmittance. The parameters are set to be homogeneous within a crown but are allowed to vary between crowns. The effect of slope is incorporated into the model using a planar surface with defined slope angle.

For LiDAR simulation, the model calculates the probability distribution of return of a photon emitted from the laser as a function of time, and has been compared with field and satellite observations (North et al., 2010; Rosette et al., 2010; Morton et al., 2014).

2.2. LUT-Based Inversion

Inverting the LiDAR waveform model was performed using a LUT approach to allow an efficient retrieval of the range of parameters possible for a given waveform. The LUT inversion requires two stages. Firstly, prior to inversion, we use the FLIGHT model to generate the LUT. Each entry in the LUT contains a waveform, and the corresponding biophysical parameter set which gave rise to that waveform. Secondly, during operation of the inversion, we automatically select from the LUT the solution or solutions whose simulated waveform in the LUT best matches to a given observed waveform.

4

The LUT was generated by modelling LiDAR waveforms, representing a total of 107100 unique canopy representations. For each: a combination of LUT parameter values was selected from within a defined range, a corresponding 3D representation of a forest stand was simulated and photon paths modelled. Values for leaf reflectance and transmittance were derived from the LIBERTY model (Dawson et al., 1998, 2003) based on field measurements of leaf structure and pigmentation from the BOREAS campaign (Hall, 1999; Plummer and Curran, 1998), while understory reflectance was based on field measurements from this campaign (Hall et al., 2000). Sensor configuration and location were fixed to appropriate GLAS specifications. The set of parameters defining the LiDAR sensor are listed in Table 1, along with example values for GLAS (Brenner et al., 2003).

Table 1: FLIGHT LiDAR sensor model and GLAS specific values.

Parameter	Description	Unit	Value
(P_x, P_y, P_z)	Sensor position relative relative to scene	m	(0, 0, 600000)
θ_o	Sensor zenith angle	deg	0
ϕ_o	Sensor azimuth angle	deg	0
s_l	RMS pulse width	ns	5
q_T	Half width angle of beam divergence	rad	0.00011
$IFOV$	Detector IFOV	rad	0.0004
A_T	Detector telescope area	m^2	0.709
$T_{RT stm}$	Roundtrip atmosphere transmittance	–	0.8 (532 nm) 0.9 (1024 nm)
E_{trans}	Total pulse energy	mJ	32 (532 nm) 72 (1024 nm)
Δ_t	Recording bin width	ns	1

Tree crowns were modelled as ellipsoidal. Horizontal tree positioning within a scene was random and tree heights were uniformly distributed between a specified minimum and maximum height range. The LUT was designed to contain a wide range of possible tree height arrangements, including stands with highly variable heights (i.e. the maximum range H_{min}–H_{max} is large) and stands with a single height canopy (i.e. the maximum range H_{min}–H_{max} is 1 m). While a single layer canopy is used here, more complex structures, for example to include an understory layer, are possible with the same methodology.

A subset of FLIGHT parameters, comprising leaf area index LAI, fractional cover F_c, lower limit height of first branch H_{min}, upper limit height of first branch (H_{max}), slope (S_y), canopy radius (E_{xy}) and for the ellipsoidal crowns used in this study, canopy radius in the vertical axis (E_z), was chosen for the LUT variables to ensure that a sufficiently broad range of stand height and coverage could be simulated. Slope referred to the angle from horizontal, of a flat

Table 2: FLIGHT parameters and ranges treated as variables for the generation of the LUT. Additional parameters (e.g. leaf optical properties and angular distribution) were fixed to default, broadleaf canopy, settings.

Parameter	Description	Unit	Min	Max	Step
LAI	Mean one-sided foliage area per unit area	$m^2 m^{-2}$	0.4	6.1	0.1
H_{max}	Maximum height to first branch	m	1	17	2
H_{min}	Minimum height to first branch	m	0	16	2
F_c	Fraction of ground covered by vegetation	%	20	80	10
S_y	Ground slope	$deg.$	0	20	5
E_{xy}	Crown horizontal radius	m	1	4	1
E_z	Crown vertical radius	m	2	8	2

plane, and is assumed to mean 'equivalent slope', and relates to the average change in elevation within a GLAS footprint. It is not possible to differentiate between localised surface roughness and footprint scale changes in elevation. The parameter ranges used are listed in Table 2. The remaining FLIGHT parameters were fixed to default values. The LUT generated using these parameters reflects a simplified representation of natural forest structures and as such the robustness and accuracy of this investigation can only be considered as an indication of the ability of this approach to retrieve accurate forest biophysical parameters.

The solution of the model inversion was then found by ranking the distance using a Chi-Square metric (χ^2) between a reference waveform (ω_{ref}) provided by GLAS and a simulated waveform (ω_{sim}) from the LUT as modelled by FLIGHT. To ensure equivalence, both waveforms were normalised by total waveform energy. A merit function was adopted:

$$\chi^2 = \sum_{i=1}^{n_{bin}} \left(\frac{\omega_{ref}[i] - \omega_{sim}[i]}{\sigma_n} \right)^2 \tag{1}$$

where n_{bin} is the number of bins of the waveform. The estimated total uncertainty for each bin σ_n is the total sum of uncertainties arising from errors (σ_{model}) such as those in the model physics and real world representation (e.g. a turbid medium approximation, vertical distribution of LAI), deviation from values of default parameters (e.g. leaf reflectance, soil reflectance), combined with the estimated measurement errors ($\sigma_{measure}$) associated with the data. The measurement and model errors are described in further detail in the following section.

$$\sigma_n^2 = \sigma_{measure}^2 + \sigma_{model}^2 \tag{2}$$

2.3. Error Estimates

A practical estimate of model error σ_{model} under real conditions was made empirically, derived from the error in model fit for a set of 66 GLAS waveforms over Forest of Dean, UK, which comprises a range of of mixed broadleaf and coniferous forest species on sloping ground (Rosette et al., 2008b). A full description of the Forest of Dean site is given in Section 3. Errors were approximated as following a Gaussian distribution, and explaining the deviation between GLAS waveform and FLIGHT model waveform as the combination of model and measurement error, after finding of the best model fit to each waveform. An estimated measurement error $\sigma_{measure}$, for each waveform was calculated as the standard deviation of the 'noise' from a non-signal portion of the waveform. Considering the reduced Chi-Square (χ^2_{red}):

$$\chi^2_{red} = \frac{\chi^2}{\nu} \tag{3}$$

where ν is Degrees of Freedom given by $N - n - 1$, where N is total number of observations, and n is the number of fitted parameters. If $\chi^2_{red} \approx 1$ indicates a good model fit, then $\chi^2 \approx \nu$.

If σ_n is assumed to be constant for all samples then an estimate for $\sigma_n = \sigma$ can be determined empirically for each waveform of a set of data from (1). Using:

$$\sigma^2 = \frac{1}{\nu} \sum_{i=1}^{n_{bin}} \left(\omega_{ref}[i] - \omega_{sim}[i] \right)^2 \tag{4}$$

Consequently, an estimate for σ^2_{model} was obtained from each waveform fit of the reference data set by (2). The underlying assumption is that the closest model fit to the 'true' forest structure has been found by the inversion, and (2) gives an approximation of the total remaining (non-parameter) error σ^2_{model} including model physics, errors in unknown/default variables such as ground reflectance, and quantisation in the LUT.

Using the Forest of Dean data as a reference data set an estimate for σ_{model} was found to be ≈ 0.001 Normalised Intensity (I_N). Subsequent analysis on all data sets: simulated, Forest of Dean (FOD), Southern Old Aspen (SOA) and Norunda (NOR) data sets included this previously determined σ_{model} alongside a measurement error $\sigma_{measure}$ estimated from the non-signal region of the waveform being analysed.

To account for the ill-posed nature of the model inversion, where a number of possible solutions may exist due to measurement or model uncertainties, the LUT was ranked according to a metric χ^2. The first $n = 1, 10, 100$ simulated waveforms were accepted to be candidate solutions and the mean of each of the parameters was considered the solution.

3. Validation Data

3.1. Forest Sites

Three sites were selected for validation of the method: a mixed temperate forest site within Forest of Dean (FOD), UK, the Southern Old Aspen Site (SOA), Saskatchewan (Canada) and a boreal coniferous site in Norunda (NOR),

Sweden. These sites were chosen to provide a range of temperate and boreal forest types, and as they have been well characterised using coincident ALS data and field survey for regions overlapping with GLAS tracks. Key characteristics for the three study sites are summarised in Table 3.

Sources of uncertainty to consider include errors in the reference ALS data. Andersen et al. (2006) aimed to quantify the accuracy of tree height measurements made using ALS over conifer study sites and found that accuracy was influenced by point density as determined by beam divergence. For a nominal 6 p/m[1] the negative bias in height retrieval was found to be -0.73 m (SD = 0.43 m) for the narrow beam (0.33 m diameter footprint) LiDAR and -1.12 m (SD = 0.56 m) for wider beam (0.8 m). In a previous study Gaveau and Hill (2003) attempted a similar study, this time for broadleaf woodland. They reported a negative bias of 1.12 m for tree height but also note that converting point data into grid format CHM data further propagated error, resulting in a negative bias of 2.12 m (RMSE = 1.89 m). Canopy cover reference data was also derived from ALS data. However, Rosette et al. (2009) showed that a good relationship with field based estimates was possible, despite a relatively small data range. Testing ALS estimates of fractional cover with hemispherical photography they found R^2 = 0.77 and RMSE = 0.02. A second source of error pertaining to the reference data may be attributed to the use of a slightly different approach for the derivation of parameters from FOD data to that used for the SOA and NOR reference data. At the time of the investigation only these derived parameters were available.

It should be noted that the Norunda site was subject to a considerable difference in time between the acquisition of the GLAS data (2003) and the airborne LiDAR data (2011). Many of the Norunda height parameter estimates were affected by vegetation growth occurring between the two data set acquisition dates. In the case of the fractional cover, land cover differences through forestry activities such as harvesting or thinning may also explain a number of overestimated outlier points.

3.1.1. Forest of Dean

The first study site was located in The Forest of Dean (FOD), Gloucestershire, UK. The forest covers an area of approximately 11,000 ha and is managed by the Forestry Commission of Great Britain. The site comprises mixed temperate species, mainly: Norway spruce (*Picea abies*), oak (*Quercus spp.*), Corsican pine (*Pinus nigra var maritima*), Douglas fir (*Pseudotsuga menziesii*), Scots pine (*Pinus sylvestris*) and European larch (*Larix decidua*).

Airborne LiDAR data were used as a proxy for ground truth data. Airborne data for the Forest of Dean study site were acquired during August 2006, using the Optech Airborne Laser Terrain Mapper (ALTM-3033) sensor system. The aerial survey was carried out by the the Natural Environment Research Council Airborne Research and Surveying Facility (ARSF) (through the Unit for Landscape Modelling, University of Cambridge), on behalf of the Forestry Commission of Great Britain Forest Research Agency.

For FOD airborne LiDAR data, the log ASCII standard (LAS) format data were processed by Rosette et al. (2008b) using the method described by Streutker and Glenn (2006). Return points were classified into vegetation and ground classes and a ground surface model was interpolated using Delaunay triangulation. Mean footprint slope was derived

8

Table 3: Characteristics of forest sites used for validation.

	FOD	SOA	NOR
Region	Forest of Dean, Great Britain	Saskatchewan, Canada	Norunda Common, Sweden
Location	51.81° N, 2.52° W	53.63° N, 106.20° W	60.09° N, 17.48° E
Elevation above sea level (m)	50–225	524–572	34–83
Topography	Moderate relief	Low relief	Low relief
Main species	Norway spruce (*Picea abies*), Oak (*Quercus spp.*), Corsican pine (*Pinus nigra*), Douglas fir (*Pseudotsuga menziesii*), Scots pine (*Pinus sylvestris*), European larch (*Larix decidua*)	Trembling aspen (*Populus tremuloides*), Hazelnut (*Corylus cornutta*)	Norway spruce (*Picea abies*), Scots pine (*Pinus sylvestris*)
Max canopy height (m)	30	21	28

from the surface model. Fractional cover (F_c) estimates were calculated as the fraction of vegetation class point count over the total point count. Only vegetation points over 0.5 m above the interpolated ground surface were counted such that, only canopy and taller understory affecting GLAS waveform were included in the observed fractional cover. Maximum canopy height within each airborne LiDAR subset was then calculated to allow a comparison to be made with estimated ICESat/GLAS height parameter.

3.1.2. Saskatchewan

The second study site is located within the southern boreal forest of Saskatchewan, Canada. The Southern Old Aspen (SOA) site was first established as part of the Boreal Ecosystem Research and Monitoring Site (BERMS) study (Barr et al., 2004, 2006; Black et al., 1996; Kljun et al., 2007) and lies approximately 10 km north of the transition zone between agriculture and forest. Located near the southern end of the Prince Albert National Park, the SOA site (Barr et al., 2004, 2006; Black et al., 1996; Chasmer et al., 2011) is predominately uniformly aged trembling aspen (*Populus tremuloides* Michx.) with hazelnut (*Corylus cornutta* Marsh) dominating the under storey (Barr et al., 2006). The terrain is mainly flat, with a site mean slope of $\approx$ 2° (Mahoney et al., 2014) and the $\approx$ 21 m stand height is relatively even due to natural regeneration after a wildfire in 1919 (Blanken et al., 1997; Amiro et al., 2006; Kljun et al., 2007). Airborne LiDAR data covering the SOA site were acquired on behalf of the authors in August 2008, by the Applied Geomatics Research Group (AGRG) and the Canadian Consortium for LiDAR Environmental Applications Research (C-CLEAR), using an Optech ALTM-3100 system.

3.1.3. Norunda

A third study site is located at Norunda (NOR) (Lindroth et al., 1998; Feigenwinter et al., 2010; Lagergren et al., 2005), situated 30 km north of Uppsala, Sweden. The site is at the southern part of the boreal forest zone and is part of the integrated carbon observation system (ICOS Sweden) research infrastructure. Norway spruce (*Picea abies*) and Scots pine (*Pinus sylvestris*) dominate the site, while there is a smaller fraction of deciduous vegetation (approximately 15%), predominately birch (*Betula sp.*) (Lindroth et al., 1998). The area is generally flat with some localised variations in elevation less than 10 m. Corresponding airborne data were acquired in June 2011 by the ARSF on behalf of the authors. A Leica ALS50-II LiDAR instrument was used.

For both the Southern Old Aspen and Norunda sites, airborne LiDAR data were processed by Chasmer et al. (2011); Mahoney et al. (2014); Kljun et al. (2013). Canopy height was derived using the IDW algorithm within a 2.5 m search radius of classified canopy reflections greater than 0.5 m above the ground (Hopkinson et al., 2005). Canopy fractional cover was calculated using the Beer's Law laser intensity method (Hopkinson and Chasmer, 2009).

3.2. GLAS Data

Waveform data in this study were acquired by the Geoscience Laser Altimeter System (GLAS) (Brenner et al., 2003; NSIDC, 2014). The GLAS instrument employed three Nd:YAG lasers (designated Laser 1, 2 and 3), to operate one at a time, at 1064 nm and 532 nm wavelengths. The 1064 nm pulse was used for measuring surface and dense cloud elevations, and , and the 532 nm pulse was used to measure the vertical distribution of clouds and aerosols. For this study, only the 1064 nm pulse was used. The instrument was required to operate at a nominal 600 km altitude and with a 375 microradian field of view to illuminate a footprint size of 70 ± 10 m (Brenner et al., 2003), however footprints were found to be elliptical and averaged 48 m × 102 m for Laser periods 1A through to 2C and 47 m × 57 m for the Laser periods 3A through to 3K (NSIDC, 2014). A pulse frequency of 40 Hz resulted in a distance of approximately 175 m between the spots measured centre-to-centre.

4,500,000 × 1 ns samples were collected for each transmitted 1064 nm pulse and on-board processing reduced this to 544 and 200 samples to be telemetered over ice sheet or land, and sea ice or water surface respectively. For the Laser 1a and 2a periods, this was designed to yield a range window of 81.6 m for land and ice sheet or 30 m for water surface (Schutz et al., 2005). However, the on-board software truncated the signal from the upper part of tall vegetation or particularly steep slopes and so for later operational periods a compression scheme was introduced to increase the overall land height range to 150 m (lower 392 bins at 1 ns = 58.8 m, upper 152 bins at 4 ns = 91.2 m) (Harding and Carabajal, 2005).

All waveform data used in the study were from the level one (L1A) GLA01 product (Zwally et al., 2011) which comprise the raw altimetry data as transmitted from the space vehicle, and includes the long (544 or 1000 bin) and short (200 bin) waveforms. Waveform footprint geolocation data were taken from the GLA14 product (Zwally et al., 2014). Footprint geolocation accuracy was known to be < 1 m for data releases V026 and onwards.

₂₅₄ Forest of Dean data were taken from release V026, and were acquired on 22nd October 2005 (laser 3D, Id:

₂₅₅ 885917496, 885917506, 885917516). The original dataset included 86 overpass footprints, but filtered to a set of 66

₂₅₆ to avoid artificial objects such as buildings and roads (Rosette et al., 2008b). For the Southern Old Aspen site, 22

₂₅₇ footprints of GLAS data were available from release V031, acquired 21st February 2003. The laser period was laser

₂₅₈ 1A. Historical weather data records from Environment Canada indicate that there was approximately 23 cm snow

₂₅₉ cover on the date of the GLAS data acquisition (Environment Canada, Government of Canada, 2014). A total of 99

₂₆₀ GLAS footprints for the Norunda study site data were acquired over two dates: 49 footprints on 22nd February 2003

₂₆₁ (laser 1A, Id: 22494495) and 50 footprints on 25th September 2003 (laser 2A, Id: 115682811), both from release

₂₆₂ V033.

₂₆₃ *3.3. Converting Fractional Cover to Projected Cover*

₂₆₄ The standard FLIGHT model output within the LUT of *fractional cover* (F_c) is defined as vertically projected total

₂₆₅ crown cover. A further LUT entry P_c is derived to approximate fractional cover compatible with airborne LiDAR, of

₂₆₆ vertically projected foliage area for tree crowns. This is calculated using the conversion formula:

$$P_c = F_c \left(1 - e^{-k\left(\frac{LAI}{F_c}\right)} \right) \tag{5}$$

₂₆₇ was used, where *k* was chosen to be 0.5.

4. Results

₂₆₉ *4.1. Sensitivity analysis*

₂₇₀ The model inversion was applied first to a simulated data set to determine the ability to retrieve parameters from

₂₇₁ individual waveforms and assess likely error. A set of 1000 waveforms representing a range of forest canopy re-

₂₇₂ alisations were created by running FLIGHT. Canopy parameters were sampled randomly within a subset of ranges

₂₇₃ specified in Table 4.

₂₇₄ R^2, MAE and bias for all solution-set sizes are summarised in Table 5. For the simulated data set, fractional cover

₂₇₅ and height were well estimated with high R^2 (0.77 and 0.91, respectively) and low mean absolute errors (MAE) (6.30

₂₇₆ % and 1.30 m, respectively). Scatterplots with the distribution of results are shown in Figures 1a and 1b. Furthermore,

₂₇₇ close proximity to the 1:1 line demonstrate the potential of this method to retrieve height. For the retrieval of canopy

₂₇₈ vertical radius, R^2 and MAE (0.77 and 0.96 m, respectively) are reasonable (Figure 1c). However, relatively large

₂₇₉ standard deviations in individual estimates indicate a higher degree of uncertainty in estimates for this parameter. A

₂₈₀ very high $R^2 = 0.93$ for slope estimation (see Figure 1d) provides further evidence to suggest that the LUT method

₂₈₁ might be suitable for estimating topography simultaneously with other forest parameters. Low variability within the

₂₈₂ solution sets is evident from the low standard deviation.

11

Table 4: FLIGHT parameters and ranges treated as variables for the generation of waveforms representing the forest canopy realisations belonging to the simulated data set. Additional parameters were fixed to the same default settings as with the generation of the LUT.

Parameter	Description	Unit	Min	Max
LAI	Mean one-sided foliage area per unit area	$m^2 m^{-2}$	2.0	6.0
H_{min}	Min height to first branch	m	0.0	16.0
H_{max}	Max height to first branch	m	0.0	17.0
F_c	Fraction of ground covered by vegetation	%	20	80
S_y	Ground slope	$deg.$	0	20
E_{xy}	Crown horizontal radius	m	2.0	4.0
E_z	Crown vertical radius	m	2.0	6.0

Table 5: Chi-Square summary statistics on simulated dataset, for solution sizes $n = 1, 10, 100$.
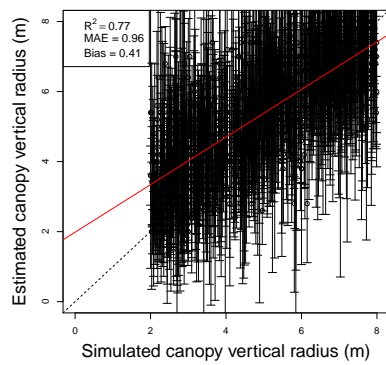
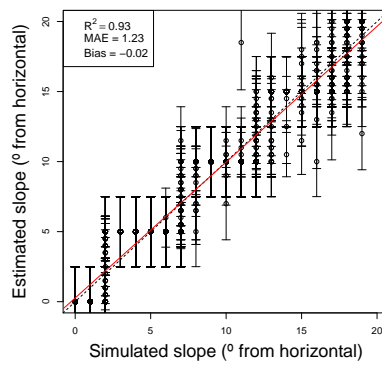| Parameter		Chi-Square		
		$n = 1$	$n = 10$	$n = 100$
H_{top}	R^2	0.81	0.91	0.91
	MAE	1.66	1.30	1.43
	Bias (m)	0.54	0.69	0.94
F_c	R^2	0.70	0.77	0.79
	MAE	7.42	6.30	5.84
	Bias	2.01	2.03	2.15
E_z	R^2	0.70	0.77	0.79
	MAE	1.26	0.96	1.00
	Bias (m)	0.38	0.41	0.55
S_y	R^2	0.91	0.93	0.94
	MAE	1.44	1.23	1.11
	Bias (deg.)	0.01	-0.02	0.00
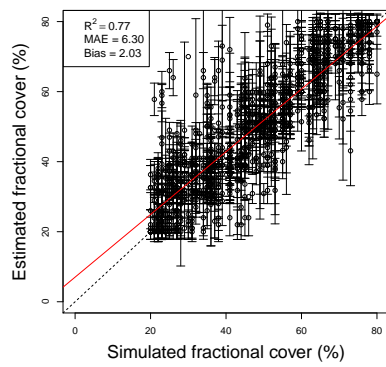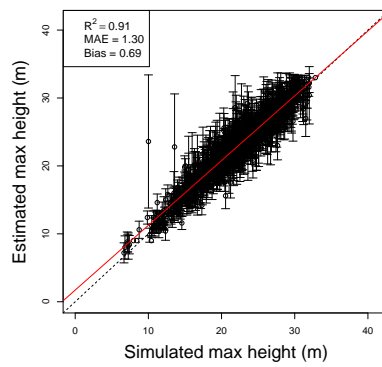
Figure 1: Chi-Square parameter estimates against FLIGHT model input parameters for simulated dataset with $n = 10$: a) Fractional cover, b) Maximum height, c) Canopy vertical radius, d) Slope. Circles represent the mean of possible set of size n solutions, and error bars represent the uncertainties related to the model inversion and are given by the standard deviation of the set of n possible solutions.

4.1.1. Response to Signal and Model Parameter Error

To investigate the effect of signal noise and error in assumed model parameters on the robustness of parameter estimation, a subset of FLIGHT parameter values were modified individually, and in combination, and the resulting simulated waveforms were compared against the LUT using the method described previously. Leaf and soil reflectance parameter values were perturbed by ±10%, and leaf diameter was set randomly to a value between 0.01–0.1 m. Waveforms simulated with combined leaf and soil noise perturbations were generated by varying randomly the reflectance parameters between ±10%. Two further LAD functions representing erectophile and planar foliage structures were specified and simulated waveform data sets were modelled accordingly; all other parameters were fixed between the three LAD types. R^2, MAE and bias for solution-set size $n = 10$ are summarised in Tables 6 and 7.

As was expected, noise added to the leaf and soil reflectance FLIGHT parameters had a greater effect on the estimation of F_c and E_z than on parameters concerning the vertical dimension e.g. H_{top} and S_y. In particular, negative bias for F_c was found to occur when leaf reflectance was decreased or when soil reflectance was increased. Conversely, bias moved in a positive direction when leaf reflectance was increased or when soil reflectance was decreased. Noise from the soil reflectance perturbation had the greatest effect on the estimation of the parameters, particularly when soil reflectance was increased. In this case, R^2 was degraded for both F_c and H_{top}. Leaf diameter noise was found to have minimal effect on forest parameter retrieval, due to the compensatory effect of the F_c and *LAI* parameters.

Table 6: Simulated: Chi-Square summary statistics of the simulated data set with added noise for leaf and soil reflectance and for leaf size, for solution size $n = 10$.

Parameter		Default	Noise					
			Leaf Spec. (−10%)	Leaf Spec. (+10%)	Soil Spec. (−10%)	Soil Spec. (+10%)	Leaf Dia. (0.01–0.1 m)	Combined
E_z	R^2	0.77	0.74	0.78	0.76	0.66	0.77	0.68
	MAE	0.96	0.99	0.96	0.84	1.26	0.96	1.03
	Bias (m)	0.41	0.37	0.49	0.13	0.87	0.42	0.51
F_c	R^2	0.77	0.74	0.78	0.76	0.66	0.77	0.68
	MAE	6.30	6.52	7.16	10.45	8.75	6.34	7.64
	Bias	2.03	-0.42	4.65	9.52	-5.23	1.94	0.47
H_{top}	R^2	0.91	0.89	0.91	0.92	0.81	0.91	0.88
	MAE	1.30	1.38	1.30	1.11	2.08	1.29	1.49
	Bias (m)	0.69	0.79	0.68	0.12	1.55	0.71	0.92
S_y	R^2	0.93	0.94	0.93	0.93	0.94	0.94	0.93
	MAE	1.23	1.20	1.26	1.25	1.24	1.20	1.26
	Bias (deg.)	-0.02	-0.19	0.21	-0.10	0.34	-0.03	0.10

14

Table 7: Simulated: Chi-Square summary statistics of the simulated data set for the three LAD classes, for solution sizes $n = 10$.

	Parameter	Spherical (Default)	Erectophile	Planar
H_{top}	R^2	0.91	0.90	0.92
	MAE	1.30	1.39	1.15
	Bias (m)	0.69	0.84	0.41
F_c	R^2	0.77	0.72	0.80
	MAE	6.30	6.79	9.77
	Bias	2.03	-0.80	9.10
E_z	R^2	0.77	0.72	0.80
	MAE	0.96	1.02	0.88
	Bias (m)	0.41	0.52	0.02
S_y	R^2	0.93	0.94	0.93
	MAE	1.23	1.21	1.21
	Bias (deg.)	-0.02	0.00	0.07

4.2. Validation of GLAS Retrievals Over Forest Sites

The model inversion was validated using spatially consistent GLAS and airborne LiDAR data from the three forest sites. A χ^2 metric was applied to every canopy realisation within the LUT and sets of various sizes of possible solutions were then selected. Estimates for canopy maximum height (H_{top}) and fractional cover (F_c) parameters were compared for all sites, while slope was additionally compared for the Forest of Dean study site. These parameters were derived from the mean of the given set of possible solutions for each waveform. Associated uncertainties were indicated by the standard deviations of the solution sets. Where the uncertainty was found to be less than the LUT parameter increment, the LUT parameter increment was used instead as the minimum uncertainty.

Representative examples of waveform fitting over the simulated and three real forest datasets are shown in Figures 2, 3, 4 and 5 and show a close agreement between the GLAS and simulated (LUT) waveforms. The typical bimodal waveform is apparent in most of the examples, however Figures 2b and 3c also show the effect of coincident vegetation and ground portions of the waveform due to the combination of topographic slope and low lying vegetation.

4.2.1. Forest of Dean

Retrieved fractional cover and height from GLAS for the Forest of Dean site are shown plotted against corresponding measurements from ALS in Figures 6a and 6b respectively, and Table 8 shows the Forest of Dean site R^2, MAE and Bias for three values of n. Fractional cover is estimated with R^2 of 0.52 and low MAE of approximately
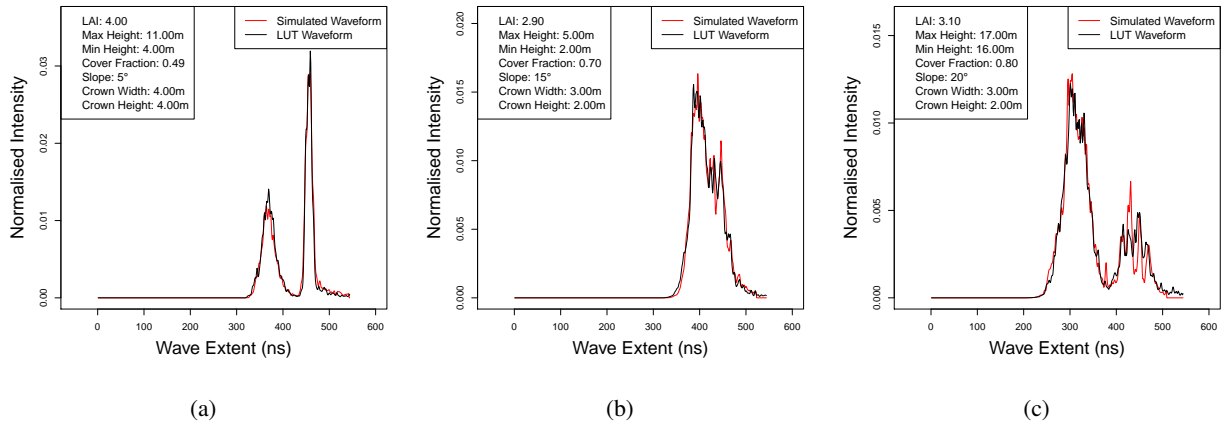
15

Figure 2: Simulated: Chi-Square metric waveform fit examples, showing best LUT fit against examples of simulated GLAS waveforms.
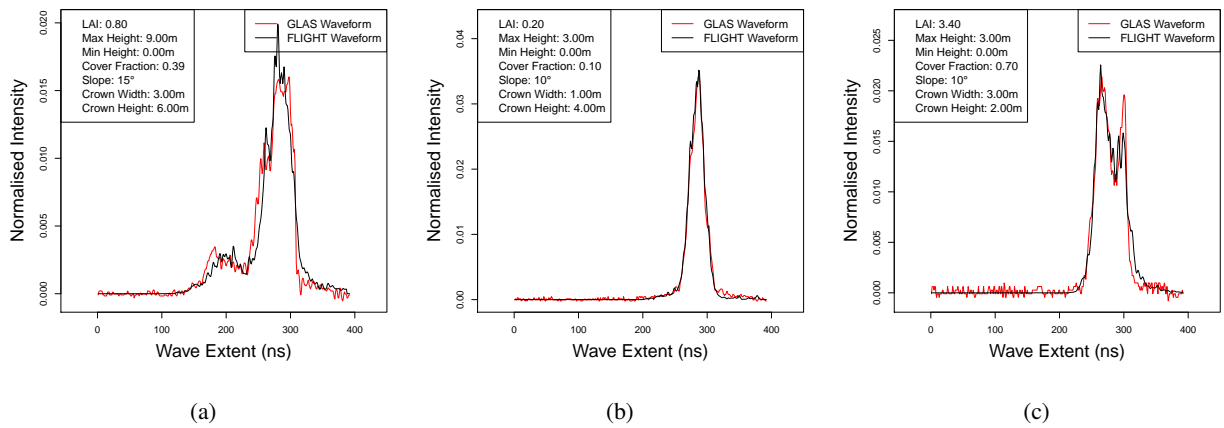

Figure 3: Forest of Dean: Chi-Square waveform fit examples, showing best LUT fit against Forest of Dean GLAS waveform examples.
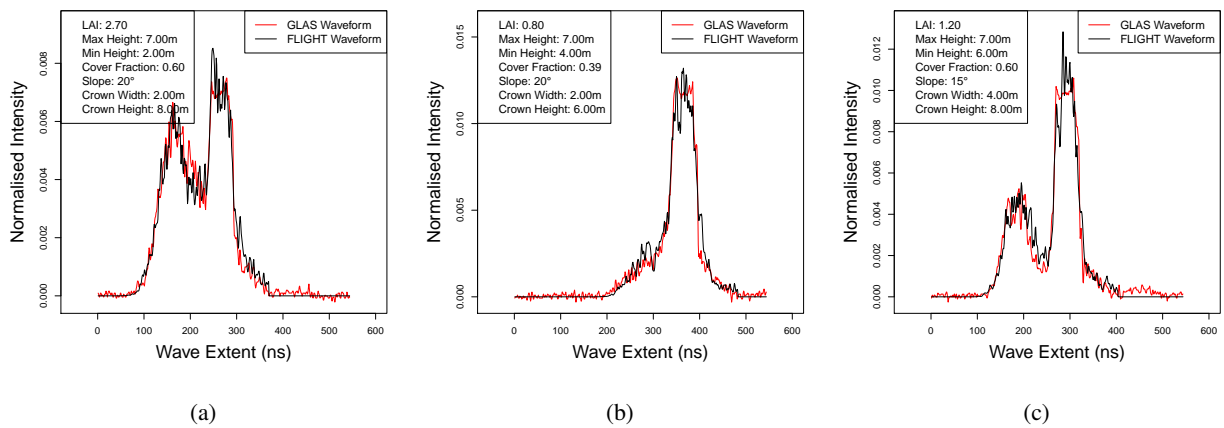

Figure 4: Southern Old Aspen: Chi-Square waveform fit examples, showing best LUT fit against Southern Old Aspen GLAS waveform examples.
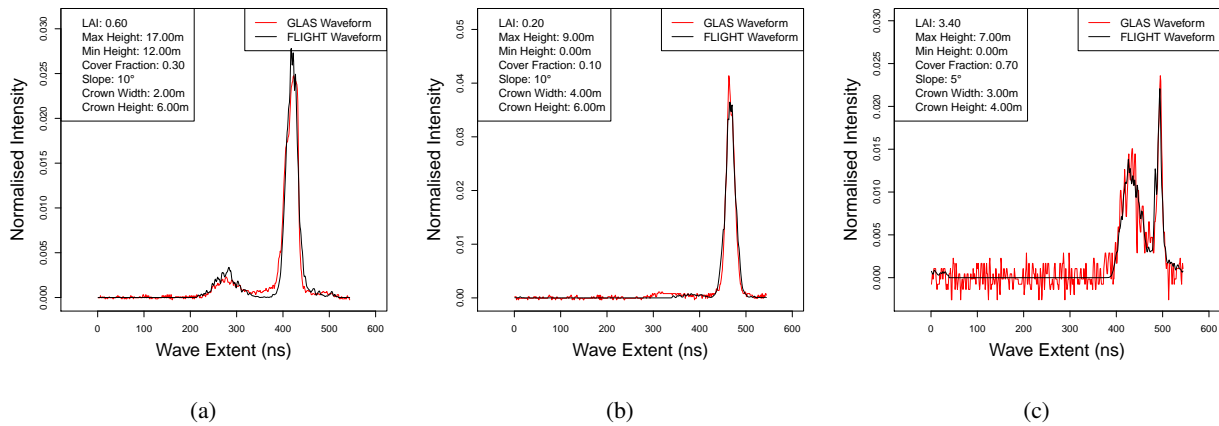
16

Figure 5: Norunda: Chi-Square waveform fit examples, showing best LUT fit against Norunda GLAS waveform examples.

0.10. Height was estimated with a high coefficient of determination ($R^2 = 0.74$) and low MAE of 3.71 m. The coefficients of determination give an indication of ability to distinguish within-site variability of height and fractional cover. Both parameters display good adherence to the 1:1 line. The Forest of Dean ICESat/GLAS and airborne data sets were acquired in closest temporal coincidence of the three datasets and the parameter regression results demonstrate robust retrieval of height and vegetation cover in this case. Ground slope is estimated with good accuracy ($MAE \leq 4°$ degrees) but showing a positive bias of $\approx 3.4°$ degrees.

4.2.2. Saskatchewan

Canopy fractional cover and height jointly derived from GLAS footprints, compared with those from ALS for the Southern Old Aspen study site are shown in figures 7a and 7b. It is important to note the model inversions were performed on the available GLAS data, which were acquired during 'leaf-off' conditions (February), while ALS fractional cover are made during a 'leaf-on' period (August). Quantitative comparison for fractional cover is not appropriate therefore, other than to note the results show an expected lower value for leaf-off, and no significant correlation. Since the conditions are very different to those assumed in the LUT (bare ground, 'leaf-on') this provides a challenging test for model inversion for other structural parameters. It is interesting to note that canopy maximum height derived from GLAS by model inversion was nevertheless estimated as close to the 1:1 line, with MAE of only 3.35m. The R^2, MAE and Bias for all solution-set sizes are summarised in Table 9.

4.2.3. Norunda

The final study site, Norunda, was subject to a considerable difference in time between the acquisition of the GLAS data (2003) and the airborne LiDAR data (2011). Figure 8b shows most points have lower values in height parameter retrieval from GLAS, compared to the later ALS data. These are likely due to growth occurring between the two data set acquisition dates. Land cover differences through natural disturbance, growth or forestry activities

17
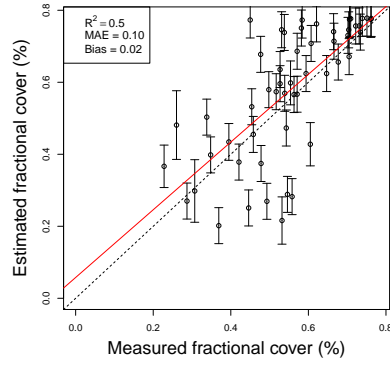
(a)
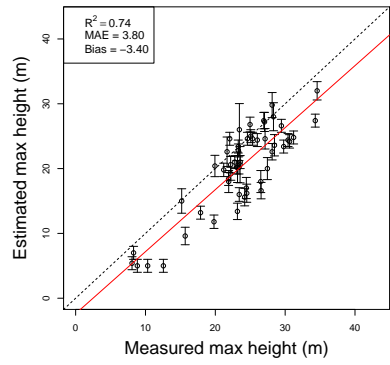
(b)
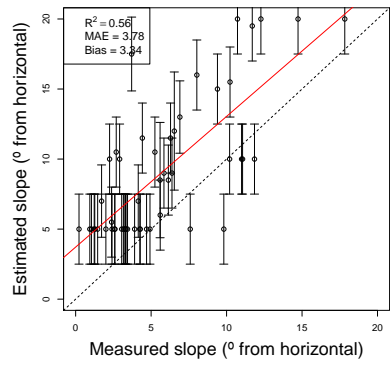
(c)

Figure 6: Forest of Dean: Chi-Square parameter estimates against airborne LiDAR derived parameters: a) Fractional cover, b) Maximum height, c) Slope. Circles represent the mean of possible set of size *n* solutions, and error bars represent the uncertainties related to the model inversion and are given by the standard deviation of the set of *n* possible solutions.

Table 8: Forest of Dean: Chi-Square summary statistics for solution sizes $n = 1, 10, 100$.

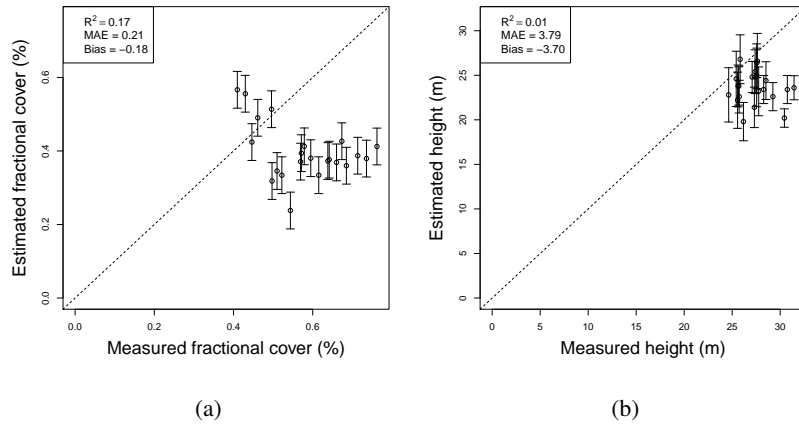| Parameter		Chi-Square		
		$n = 1$	$n = 10$	$n = 100$
	R^2	0.71	0.74	0.70
H_{top}	MAE	4.00	3.80	3.71
	Bias (m)	-3.53	-3.40	-3.26
	R^2	0.51	0.50	0.52
F_c	MAE	0.10	0.10	0.10
	Bias (m)	0.02	0.02	0.01
	R^2	0.57	0.56	0.54
S_y	MAE	3.74	3.78	4.19
	Bias (deg.)	3.29	3.34	3.87

Figure 7: Southern Old Aspen: Chi-Square estimated parameters against airborne LiDAR derived parameters: a) Fractional cover, b) Maximum height. Circles represent the mean of possible set of size n solutions, and error bars represent the uncertainties related to the model inversion and are given by the standard deviation of the set of n possible solutions.

Table 9: Southern Old Aspen: Chi-Square summary statistics for solution sizes $n = 1, 10, 100$. Parameter S_y was left out of analysis as elevation change within the GLAS footprint was insignificant.

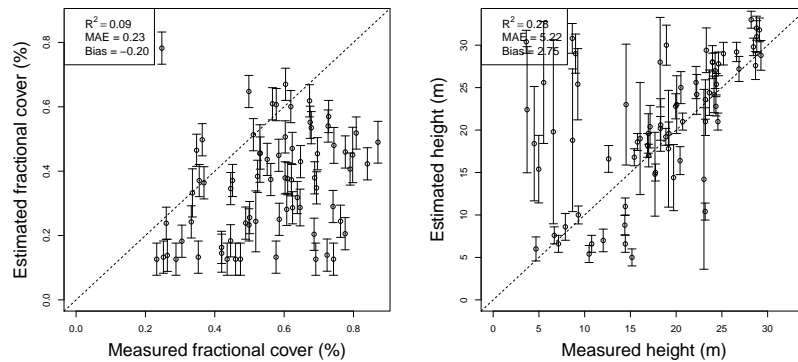| Parameter		Chi-Square		
		$n = 1$	$n = 10$	$n = 100$
	R^2	0.00	0.01	0.07
H_{top}	MAE	4.36	3.97	3.35
	Bias (m)	-4.23	-3.70	-3.25
	R^2	0.34	0.17	0.10
F_c	MAE	0.22	0.21	0.20
	Bias	-0.19	-0.18	-0.18

Table 10: Norunda: Chi-Square solutions summary statistics for solution sizes $n = 1, 10, 100$. Parameter S_y was left out of analysis as elevation change within the GLAS footprint was insignificant.

Parameter		Chi-Square		
		$n = 1$	$n = 10$	$n = 100$
	R^2	0.16	0.28	0.24
H_{top}	MAE	6.00	5.22	5.13
	Bias	2.77	3.75	3.39
	R^2	0.10	0.09	0.13
F_c	MAE	0.23	0.23	0.24
	Bias	-0.20	-0.20	-0.22

such as clear felling and thinning also explain a number of overestimated outlier points for both height and fractional cover. As a result the MAE in height is somewhat higher for this comparison (5.13 m) than the first two examples. Fractional cover estimates show reasonable MAE (0.23), but low coefficient of determination, suggesting noise is high compared to within-site variability. Although making evaluation of retrieval accuracy more difficult, the large number of explained outlier points compared to other two sites, which did not experience significant growth or management, suggest the the method may be well suited to monitoring changes in height and vegetation cover over time. The R^2, MAE and Bias for all solution-set sizes are summarised in Table 10.

5. Discussion

The inversion of the waveform LiDAR model using the LUT method provided estimates for the maximum canopy height for the Forest of Dean, Saskatchewan and Norunda sites. MAE was determined to be: 3.80 m, 3.35 m, 5.13 m, respectively. ALS derived height estimate uncertainty bounds are well within those found using this method. An

20

(a) Fractional cover estimated using the weighted Chi-Square metric with $n = 10$.

(b) Maximum height estimated using the weighted Chi-Square metric with $n = 10$.

Figure 8: Norunda: Chi-Square estimated parameters against airborne LiDAR derived parameters: a) Fractional cover, b) Maximum height. Circles represent the mean of possible set of size n solutions, and error bars represent the uncertainties related to the model inversion and are given by the standard deviation of the set of n possible solutions.

347 ability to detect the available within-site variability is shown by the R^2 values of: 0.74, 0.07, 0.30, respectively.

348 Maximum height was best estimated at the Forest of Dean and Saskatchewan sites but degraded at the Norunda

349 site. This was likely due to the temporal difference between GLAS and ALS data sets, and forestry related activity

350 at this site. Using Swedish NFI data, the GLAS were filtered to only allow footprints located in stands that were at

351 or near maturity and had not been subject to forestry activities. The filtering resulted in only three remaining points

352 and so was not considered to be a robust sample. However, bias and MAE for height was found to be 0.92 m and

353 2.75 m, respectively — a clear improvement. Accuracy for maximum canopy height was surprisingly good at the

354 Saskatchewan site, considering the height retrieval was made using GLAS data acquired during 'leaf-off' conditions,

355 where a decrease in returned energy is likely to lower the estimated maximum canopy height (Wasser et al., 2013).

356 The most commonly used height metric to derive vegetation height from GLAS LiDAR data is waveform extent,

357 defined as the height difference between the first and last elevation at which the waveform energy exceeds a threshold,

358 usually set as 4.5 times background noise (Lefsky et al., 2005, 2007). Results using the method described in our study

359 compare well to those using the former method, presented by Los et al. (2012) and Rosette et al. (2009). Los et al.

360 (2012) also additionally employ a number of filters such that up to 75% of points were removed in tropical forest

361 study sites, and validating against aircraft derived height data to achieve r = 0.67 and RMSE ≈ 8 m. Rosette et al.

362 (2009) use the same Forest of Dean GLAS and airborne LiDAR data as described in this study to obtain $R^2 = 0.68$

363 and MAE = 4.4 m for maximum canopy height when using GLAS data products.

364 A number of the height overestimates were due to the tested metric fitting noise in a GLAS waveform to a compa-

365 rably sized vegetation peak in a FLIGHT waveform representing very low fractional cover or LAI. Alternative metrics

366 may increase the accuracy of the fitting of very low intensity portions of the GLAS waveform, improving vegetation

21

signal start and end point estimations. However height estimates generally agreed with field measurements acquired by Rosette et al. (2008b), with results close to the 1:1 line.

Fractional cover was comparably well estimated for the combined dominant cover classes Forest of Dean site, (R^2 = 0.50 and MAE = 0.10). Again, ALS derived uncertainty bounds are well inside those found using the presented method. For the Norunda site, the time difference between GLAS and airborne data acquisition dates prevented a more realistic parameter estimate from being obtained. When the data set was filtered, a total of three GLAS footprints remained. From these, MAE was determined to be 0.13. For the deciduous Southern Old Aspen site, the availability of only 'leaf-off' winter GLAS data meant that it was not possible to assess fractional cover estimates.

Slope beneath canopy was retrieved for the Forest of Dean site, where within-footprint elevation changes were significant, and found to have a R^2 of 0.56 compared to airborne LiDAR measurements, but with a positive bias of 3.78°; this overestimate of slope would be expected to lead to an underestimate of canopy height equivalent to ≈ 3–4 m to explain the same total waveform extent. This was tested over an inland water surface in Norunda, where the FLIGHT LiDAR return shows a narrower return peak than the GLAS waveform, requiring an equivalent slope of 3–5° to match. The reason for the widened GLAS ground peak in real waveform returns compared to modelled is unclear. A finer granularity slope parameter range may improve the slope estimation, where quantisation in the LUT leads to a 'binning' effect (see Figure 1d) but would not correct bias. A possible reason for the systematic slope mismatch could be due to small scale surface roughness detected by GLAS but not modelled in FLIGHT. A second potential explanation for the slope underestimate is due to an apparent small but systematic underestimate in modelled waveform temporal width which is based on published instrument parameters.

Choice of optimum solution set size n was not clear from the sites investigated and varied between parameter and site. It was observed that solution set medians remained relatively similar as n increased. However, variances about the means of the solution sets were found to increase as n increased. For this study, a value $n = 10$ was chosen over $n = 1$ so that an indicator of solution uncertainty could be determined, while also minimising uncertainty around the estimated parameter. Furthermore, high values of n (e.g. $n > 1000$) significantly impact the speed of the calculations.

In addition to uncertainties due to instrument and model errors, a significant source of error was attributed to the combination of returns from both vegetation and ground elevations, that occur due to the size of the illuminated footprint and as a function of ground slope (Harding and Carabajal, 2005). Ancillary topographic information (e.g. SRTM or ASTER DEM) may provide a means to preselect LUT waveforms to significantly increase the accuracy and efficiency of retrieval (Mahoney et al., 2014). Furthermore, where this LUT used fixed values for ground and canopy reflectance, a more comprehensive LUT implementation might vary these parameters and then use methods (Armston et al., 2013; Chen et al., 2014) to derive these reflectance parameters directly from the LiDAR waveform, again for the purpose of preselecting LUT waveforms.

A third source of error can be directly attributed to the LUT design. Inspection of the waveform fit plots revealed that original choice of canopy parameters in some cases was not sufficient to span the full range found in the study sites, in particular where a lower canopy stratum could result in confusion with a ground return. Koetz et al. (2007)

also report that the good performance of their model inversion was likely due to a two strata canopy simulation within their formulation. However the approach presented here allows flexible specification of structure, allowing a wider range of parameters or easily permitting more complex structures such as row-crop or two-strata canopy structures in a LUT.

6. Conclusion

This study has developed and evaluated a new method for parameter retrieval from satellite waveform LiDAR based on inversion of the three-dimensional FLIGHT radiative transfer model. A lookup table approach is developed allowing complex canopy optical properties and multi-scale structure, instrument laser emitted signal and its return detection, to provide a physically-based simultaneous retrieval of forest structural parameters, terrain slope and their uncertainty. A sensitivity study suggested potential accuracy of retrieval of forest height from GLAS data of ≈ 1.5 m, and fractional cover of 8%.

Testing using real GLAS waveforms over three forest sites demonstrated that the method for forest canopy parameter retrieval from satellite waveform LiDAR was robust to cover type (Table 8). For the Forest of Dean site which had the nearest fitting GLAS and ALS coverage (Oct 2005 vs Oct 2006), three parameters were estimated to a high level of accuracy with height: MAE = 3.71 m; $R^2 = 0.74$, fractional cover: MAE = 0.10; $R^2 = 0.50$ and ground slope: MAE = 3.78°; $R^2 = 0.56$. This showed improvement over previous retrieval for this site using the same data as input (Rosette et al., 2009). Other sites showed good height retrieval (MAE = 3.3–5.1 m) but lower R^2 due in part to lower within-site variability compared to retrieval errors.

Results are in part dependent on the use of an appropriate LUT for the canopy being measured, although the canopy height retrieval appeared relatively robust to leaf-on/ leaf off conditions and snow vs bare ground. The method could include available ancillary information such as ground slope or vegetation type in order to optimise performance where these are known. The results suggest that the method used in this study is at least comparable to existing techniques and also offers the further advantage of being able to retrieve multiple parameters simultaneously, including sub-canopy terrain, and readily adaptable to future planned spaceborne LiDAR instruments (Dubayah et al., 2014; Montesano et al., 2015).

8. References

Abdalati, W., Zwally, H. J., Bindschadler, R., Csatho, B., Farrell, S. L., Fricker, H. A., Harding, D. J., Kwok, R., Lefsky, M., Thorsten, M., Marshak, A., Neumann, T., Palm, S., Schutz, B., Smith, B., Spinhirne, J., Webb, C., 2010. The ICESat-2 Laser Altimetry Mission. Proceedings of the IEEE 98 (5), 735–751.

Aldred, A. H., Bonner, G. M., et al., 1985. Application of airborne lasers to forest surveys. Vol. 51. Agriculture Canada, Ministry of State for Forestry.

Amiro, B. D., Barr, A. G., Black, T. A., Iwashita, H., Kljun, N., McCaughey, J. H., Morgenstern, K., Murayama, S., Nesic, Z., Orchansky, A. L., Saigusa, N., 2006. Carbon, energy and water fluxes at mature and disturbed forest sites, Saskatchewan, Canada. Agricultural and Forest Meteorology 136 (3–4), 237–251, Advances in Surface-Atmosphere Exchange - A Tribute to Marv Wesely.

Andersen, H., Reutebuch, S. E., McGaughey, R. J., 2006. A rigorous assessment of tree height measurements obtained using airborne lidar and conventional field methods. Canadian Journal of Remote Sensing 32 (5), 355–366.

Armston, J., Disney, M., Lewis, P., Scarth, P., Phinn, S., Lucas, R., Bunting, P., Goodwin, N., 2013. Direct retrieval of canopy gap probability using airborne waveform lidar. Remote Sensing of Environment 134, 24–38.

Barr, A. G., Black, T. A., Hogg, E., Kljun, N., Morgenstern, K., Nesic, Z., 2004. Inter-annual variability in the leaf area index of a boreal aspen-hazelnut forest in relation to net ecosystem production. Agricultural and Forest Meteorology 126 (3), 237–255.

Barr, A. G., Morgenstern, K., Black, T. A., McCaughey, J. H., Nesic, Z., 2006. Surface energy balance closure by the eddy-covariance method above three boreal forest stands and implications for the measurement of the CO_2 flux. Agricultural and Forest Meteorology 140 (1), 322–337.

Black, T. A., Den Hartog, G., Neumann, H. H., Blanken, P. D., Yang, P. C., Russell, C., Nesic, Z., Lee, X., Chen, S. G., Staebler, R., et al., 1996. Annual cycles of water vapour and carbon dioxide fluxes in and above a boreal aspen forest. Global Change Biology 2 (3), 219–229.

Blair, J. B., Rabine, D. L., Hofton, M. A., 1999. The laser vegetation imaging sensor: a medium-altitude, digitisation-only, airborne laser altimeter for mapping vegetation and topography. ISPRS Journal of Photogrammetry and Remote Sensing 54 (2–3), 115–122.

Blanken, P. D., Black, T. A., Yang, P. C., Neumann, H. H., Nesic, Z., Staebler, R., Den Hartog, G., Novak, M. D., Lee, X., 1997. Energy balance and canopy conductance of a boreal aspen forest: partitioning overstory and understory components. Journal of Geophysical Research: Atmospheres (1984–2012) 102 (D24), 28915–28927.

Brenner, A. C., Zwally, H. J., Bentley, C. R., Csatho, B. M., Harding, D. J., Hofton, M. A., Minster, J., Roberts, L.,

Saba, J. L., 2003. Algorithm Theoretical Basis Document 4.1: Derivation of range and range distributions from laser pulse waveform analysis for surface elevations, roughness, slope, and vegetation heights. NASA.

Calders, K., Lewis, P., Disney, M., Verbesselt, J., Herold, M., 2013. Investigating assumptions of crown archetypes for modelling lidar returns. Remote Sensing of Environment 134, 39–49.

Chasmer, L., Kljun, N., Hopkinson, C., Brown, S., Milne, T., Giroux, K., Barr, A., Devito, K., Creed, I., Petrone, R., 2011. Characterizing vegetation structural and topographic characteristics sampled by eddy covariance within two mature aspen stands using LiDAR and a flux footprint model: Scaling to MODIS. Journal of Geophysical Research: Biogeosciences (2005–2012) 116 (G2).

Chen, X. T., Disney, M. I., Lewis, P., Armston, J., Han, J. T., Li, J. C., 2014. Sensitivity of direct canopy gap fraction retrieval from airborne waveform lidar to topography and survey characteristics. Remote Sensing of Environment 143, 15–25.

Ciais, P., Sabine, C., Bala, G., Bopp, L., Brovkin, V., Canadell, J., Chhabra, A., DeFries, R., Galloway, J., Heimann, M., Jones, C., Le Quéré, C., Myneni, R. B., Piao, S., Thornton, P., 2013. Carbon and Other Biogeochemical Cycles. In: Climate Change 2013: The Physical Science Basis. Contribution of Working Group I to the Fifth Assessment Report of the Intergovernmental Panel on Climate Change. Cambridge University Press, Cambridge, United Kingdom and New York, NY, USA.

Coyle, D. B., Stysley, P. R., Poulios, D., Clarke, G. B., Kay, R. B., 2015. Laser transmitter development for NASA's Global Ecosystem Dynamics Investigation (GEDI) lidar. In: SPIE Optical Engineering+ Applications. International Society for Optics and Photonics, pp. 961208–961208.

Dawson, T. P., Curran, P. J., Plummer, S. E., 1998. LIBERTY — Modeling the effects of leaf biochemical concentration on reflectance spectra. Remote Sensing of Environment 65 (1), 50–60.

Dawson, T. P., North, P. R. J., Plummer, S. E., Curran, P. J., 2003. Forest ecosystem chlorophyll content: implications for remotely sensed estimates of net primary productivity. International Journal of Remote Sensing 24 (3), 611–617.

Disney, M., Lewis, P., Saich, P., 2006. 3D modelling of forest canopy structure for remote sensing simulations in the optical and microwave domains. Remote Sensing of Environment 100 (1), 114–132.

Drake, J. B., Dubayah, R. O., Clark, D. B., Knox, R. G., Blair, J. B., Hofton, M. A., Chazdon, R. L., Weishampel, J. F., Prince, S., 2002. Estimation of tropical forest structural characteristics using large-footprint LiDAR. Remote Sensing of Environment 79 (23), 305–319, Recent Advances in Remote Sensing of Biophysical Variables.

Dubayah, R., Goetz, S., Blair, J. B., Luthcke, S., Healey, S., Hansen, M., Hofton, M., Hurtt, G., Kellner, J., Fatoyinbo, T., et al., 2014. The Global Ecosystem Dynamics Investigation (GEDI) Lidar. In: ForestSAT2014 Open Conference System.

Duncanson, L. I., Niemann, K. O., Wulder, M. A., 2010. Estimating forest canopy height and terrain relief from GLAS waveform metrics. Remote Sensing of Environment 114 (1), 138–154.

Duursma, R., Medlyn, B., et al., 2012. MAESPA: a model to study interactions between water limitation, environmental drivers and vegetation function at tree and stand levels, with an example application to CO_2 drought interactions.

Geoscientific Model Development.

Environment Canada, Government of Canada, 2014. Historical Climate Data. `http://climate.weather.gc.ca`.

Feigenwinter, C., Mölder, M., Lindroth, A., Aubinet, M., 2010. Spatiotemporal evolution of CO_2 concentration, temperature, and wind field during stable nights at the Norunda forest site. Agricultural and Forest Meteorology 150 (5), 692–701.

Gaveau, D., Hill, R. A., 2003. Quantifying canopy height underestimation by laser pulse penetration in small-footprint airborne laser scanning data. Canadian Journal of Remote Sensing 29 (5), 650–657.

Goetz, S., Dubayah, R., 2011. Advances in remote sensing technology and implications for measuring and monitoring forest carbon stocks and change. Carbon Management 2 (3), 231–244.

Hall, F. G., 1999. Introduction to special section: BOREAS in 1999: Experiment and science overview. Journal of Geophysical Research: Atmospheres 104 (D22), 27627–27639.

Hall, F. G., Curd, S., Supronowicz, J., Edwards, G., Viau, A., Thomson, K., 2000. BOREAS TE-9 In Situ Understory Spectral Reflectance Within the NSA. Data set. Available on-line [http://www.daac.ornl.gov] from Oak Ridge National Laboratory Distributed Active Archive Center, Oak Ridge, Tennessee, USA.

Harding, D. J., Carabajal, C. C., 2005. ICESat waveform measurements of within-footprint topographic relief and vegetation vertical structure. Geophysical Research Letters 32 (21).

Harding, D. J., Lefsky, M. A., Parker, G. G., Blair, J. B., 2001. Laser altimeter canopy height profiles: methods and validation for closed-canopy, broadleaf forests. Remote Sensing of Environment 76 (3), 283–297.

Hopkinson, C., Chasmer, L., 2009. Testing LiDAR models of fractional cover across multiple forest ecozones. Remote Sensing of Environment 113 (1), 275–288.

Hopkinson, C., Chasmer, L., Sass, G., Creed, I., Sitar, M., Kalbfleisch, W., Treitz, P., 2005. Assessing vegetation height and canopy volume in a boreal wetland complex using airborne scanning LiDAR. Canadian Journal of Remote Sensing 31 (2), 191–206.

Kimes, D., Gastellu-Etchegorry, J., Esteve, P., 2002. Recovery of forest canopy characteristics through inversion of a complex 3D model. Remote Sensing of Environment 79 (2), 320–328.

Kljun, N., Black, T. A., Griffis, T. J., Barr, A. G., Gaumont-Guay, D., Morgenstern, K., McCaughey, J. H., Nesic, Z., 2007. Response of net ecosystem productivity of three boreal forest stands to drought. Ecosystems 10 (6), 1039–1055.

Kljun, N., Chasmer, L., Hopkinson, C., Lindroth, A., Mahoney, C., Mölder, M., Soudant, A., 2013. LiDAR derived canopy structure and footprint modelling for interpretation of eddy-flux tower measurements at norunda, sweden. AGU Fall Meeting Abstracts 1, 03.

Koetz, B., Morsdorf, F., Sun, G., Ranson, K. J., Itten, K., Allgower, B., 2006. Inversion of a LiDAR waveform model for forest biophysical parameter estimation. Geoscience and Remote Sensing Letters, IEEE 3 (1), 49–53.

Koetz, B., Sun, G., Morsdorf, F., Ranson, K. J., Kneubuhler, M., Itten, K., Allgower, B., 2007. Fusion of imaging spectrometer and LiDAR data over combined radiative transfer models for forest canopy characterization. Remote

Sensing of Environment 106 (4), 449–459.

Lagergren, F., Eklundh, L., Grelle, A., Lundblad, M., Mölder, M., Lankreijer, H., Lindroth, A., 2005. Net primary production and light use efficiency in a mixed coniferous forest in Sweden. Plant, Cell & Environment 28 (3), 412–423.

Lefsky, M. A., 2010. A global forest canopy height map from the Moderate Resolution Imaging Spectroradiometer and the Geoscience Laser Altimeter System. Geophysical Research Letters 37 (15).

Lefsky, M. A., Cohen, W. B., Acker, S. A., Parker, G. G., Spies, T. A., Harding, D., 1999a. LiDAR remote sensing of the canopy structure and biophysical properties of Douglas-fir western hemlock forests. Remote Sensing of Environment 70 (3), 339–361.

Lefsky, M. A., Harding, D., Cohen, W. B., Parker, G., Shugart, H. H., 1999b. Surface LiDAR remote sensing of basal area and biomass in deciduous forests of eastern Maryland, USA. Remote Sensing of Environment 67 (1), 83–98.

Lefsky, M. A., Harding, D. J., Keller, M., Cohen, W. B., Carabajal, C. C., Espirito-Santo, F. D. B., Hunter, M. O., de Oliveira Jr, R., 2005. Estimates of forest canopy height and aboveground biomass using ICESat. Geophysical Research Letters 32 (22), L22S02.

Lefsky, M. A., Keller, M., Pang, Y., de Camargo P. B., O., H. M., 2007. Revised method for forest canopy height estimation from Geoscience Laser Altimeter System waveforms. Journal of Applied Remote Sensing 1.

Leonenko, G., Los, S. O., North, P. R. J., 2013. Retrieval of leaf area index from MODIS surface reflectance by model inversion using different minimization criteria. Remote Sensing of Environment 139, 257–270.

Lindroth, A., Grelle, A., Morén, A., 1998. Long-term measurements of boreal forest carbon balance reveal large temperature sensitivity. Global Change Biology 4 (4), 443–450.

Los, S. O., Rosette, J. A. B., Kljun, N., North, P. R. J., Chasmer, L., Suárez, J. C., Hopkinson, C., Hill, R. A., Gorsel, E. v., Mahoney, C., et al., 2012. Vegetation height and cover fraction between 60 S and 60 N from ICESat/GLAS data. Geoscientific Model Development 5 (2), 413–432.

Ma, H., Song, J., Wang, J., 2015. Forest canopy LAI and vertical FAVD profile inversion from airborne full-waveform LiDAR data based on a radiative transfer model. Remote Sensing 7 (2), 1897–1914.

Mahoney, C., Kljun, N., Los, S. O., Chasmer, L., Hacker, J. M., Hopkinson, C., North, P. R. J., Rosette, J. A. B., van Gorsel, E., 2014. Slope estimation from ICESat/GLAS. Remote Sensing 6 (10), 10051–10069.

Means, J. E., Acker, S. A., Harding, D. ., Blair, J. B., Lefsky, M. A., Cohen, W. B., Harmon, M. E., McKee, W., 1999. Use of large-footprint scanning airborne LiDAR to estimate forest stand characteristics in the Western Cascades of Oregon - biomass distribution and production budgets. Remote Sensing of Environment 67 (3), 298–308.

Montesano, P. M., Rosette, J., Sun, G., North, P. R. J.and Nelson, R. F., Dubayah, R. O., Ranson, K. J., Kharuk, V., 2015. The uncertainty of biomass estimates from modeled ICESat-2 returns across a boreal forest gradient. Remote Sensing of Environment 158, 95–109.

Morton, D. C., Nagol, J., Carabajal, C. C., Rosette, J., Palace, M., Cook, B. D., Vermote, E. F., Harding, D. J., North, P. R. J., 2014. Amazon forests maintain consistent canopy structure and greenness during the dry season. Nature

506 (7487), 221–224.

Neigh, C., Nelson, R. F., Ranson, K. J., Margolis, H. A., Montesano, P. M., Sun, G., Kharuk, V., Næsset, E., Wulder, M. A., Andersen, H., 2013. Taking stock of circumboreal forest carbon with ground measurements, airborne and spaceborne LiDAR. Remote Sensing of Environment 137, 274–287.

Nelson, R., Krabill, W., MacLean, G., 1984. Determining forest canopy characteristics using airborne laser data. Remote Sensing of Environment 15 (3), 201–212.

Nelson, R., Ranson, K. J., Sun, G., Kimes, D. S., Kharuk, V., Montesano, P., 2009. Estimating siberian timber volume using MODIS and ICESat/GLAS. Remote Sensing of Environment 113 (3), 691–701.

Ni-Meister, W., Jupp, D. L. B., Dubayah, R., 2001a. Modeling LiDAR waveforms in heterogeneous and discrete canopies. Geoscience and Remote Sensing, IEEE Transactions on 39 (9), 1943–1958.

Ni-Meister, W., Jupp, D. L. B., Dubayah, R., Sep 2001b. Modelling lidar waveforms in heterogeneous and discrete canopies. IEEE Transactions on Geoscience and Remote Sensing 39 (9), 1943–1958.

North, P. R. J., 1996. Three-dimensional forest light interaction model using a Monte Carlo method. Geoscience and Remote Sensing, IEEE Transactions on 34 (4), 946–956.

North, P. R. J., Rosette, J. A., Suarez, J. C., Los, S. O., 2010. A Monte Carlo radiative transfer model of satellite waveform LiDAR. International Journal of Remote Sensing 31 (5), 1343–1358.

NSIDC, 2014. ICESat/GLAS Data. `http://http://nsidc.org/data/icesat/`.

Plummer, S. E., Curran, P. J., 1998. BOREAS RSS-04 1994 Jack Pine Leaf Biochemistry and Modelled Spectra in the SSA. Data set. Available on-line [http://www.daac.ornl.gov] from Oak Ridge National Laboratory Distributed Active Archive Center, Oak Ridge, Tennessee, USA.

Popescu, S. C., Zhao, K., Neuenschwander, A., Lin, C., 2011. Satellite LiDAR vs. small footprint airborne LiDAR: Comparing the accuracy of aboveground biomass estimates and forest structure metrics at footprint level. Remote Sensing of Environment 115 (11), 2786–2797, {DESDynI} VEG-3D Special Issue.

Rosette, J. A., North, P. R. J., Suarez, J. C., 2008a. Satellite LiDAR estimation of stemwood volume; a method using waveform decomposition. Photogrammetric Journal of Finland 21 (1).

Rosette, J. A., North, P. R. J., Suarez, J. C., 2008b. Vegetation height estimates for a mixed temperate forest using satellite laser altimetry. International journal of remote sensing 29 (5), 1475–1493.

Rosette, J. A., North, P. R. J., Suarez, J. C., Armston, J. D., 2009. A comparison of biophysical parameter retrieval for forestry using airborne and satellite LiDAR. International Journal of Remote Sensing 30 (19), 5229–5237.

Rosette, J. A. B., North, P. R. J., Suarez, J. C., Los, S. O., 2010. Uncertainty within satellite lidar estimations of vegetation and topography. International Journal of Remote Sensing 31 (5), 1325–1342.

Schutz, B. E., Zwally, H. J., Shuman, C. A., Hancock, D., DiMarzio, J. P., 2005. Overview of the ICESat mission. Geophysical Research Letters 32 (21).

Simard, M., Pinto, N., Fisher, J. B., Baccini, A., 2011. Mapping forest canopy height globally with spaceborne LiDAR. Journal of Geophysical Research: Biogeosciences (2005–2012) 116 (G4).

Streutker, D. R., Glenn, N. F., 2006. LiDAR measurement of sagebrush steppe vegetation heights. Remote Sensing of Environment 102 (1–2), 135–145.

Sun, G., Ranson, K. J., 2000. Modeling LiDAR returns from forest canopies. Geoscience and Remote Sensing, IEEE Transactions on 38 (6), 2617–2626.

Wasser, L., Day, R., Chasmer, L., Taylor, A., 2013. Influence of vegetation structure on lidar-derived canopy height and fractional cover in forested riparian buffers during leaf-off and leaf-on conditions. PLoS One 8 (1), e54776.

Weiss, M., Baret, F., Myneni, R., Pragnère, A., Knyazikhin, Y., 2000. Investigation of a model inversion technique to estimate canopy biophysical variables from spectral and directional reflectance data. Agronomie 20 (1), 3–22.

Widlowski, J.-L., Côté, J.-F., Béland, M., 2014. Abstract tree crowns in 3d radiative transfer models: Impact on simulated open-canopy reflectances. Remote Sensing of Environment 142, 155–175.

Wulder, M. A., White, J. C., Bater, C. W., Coops, N. C., Hopkinson, C., Chen, G., 2012. LiDAR plots - a new large-area data collection option: Context, concepts, and case study. Canadian Journal of Remote Sensing 38 (5), 600–618.

Xing, Y., de Gier, A., Zhang, J., Wang, L., 2010. An improved method for estimating forest canopy height using ICESat-GLAS full waveform data over sloping terrain: A case study in Changbai mountains, China. International Journal of Applied Earth Observation and Geoinformation 12 (5), 385–392.

Zwally, H., Schutz, B., Bentley, C., Bufton, J., Herring, T., Minster, J., Spinhirne, J., Thomas, R., 2011. GLAS/ICESat L1A Global Altimetry Data. Version 33. Boulder, Colorado USA: NASA National Snow and Ice Data Center Distributed Active Archive Center.

Zwally, H., Schutz, B., Bentley, C., Bufton, J., Herring, T., Minster, J., Spinhirne, J., Thomas, R., 2014. GLAS/ICESat L2 Global Land Surface Altimetry Data. Version 34. Boulder, Colorado USA: NASA National Snow and Ice Data Center Distributed Active Archive Center.